

# Aligning Task- and Reconstruction-Oriented Communications for Edge Intelligence

Yufeng Diao, *Graduate Student Member, IEEE*, Yichi Zhang, *Graduate Student Member, IEEE*,  
Changyang She, *Senior Member, IEEE*, Philip Guodong Zhao, *Senior Member, IEEE*,  
and Emma Liying Li, *Member, IEEE*

**Abstract**—Existing communication systems aim to reconstruct the information at the receiver side, and are known as reconstruction-oriented communications. This approach often falls short in meeting the real-time, task-specific demands of modern AI-driven applications such as autonomous driving and semantic segmentation. As a new design principle, task-oriented communications have been developed. However, it typically requires joint optimization of encoder, decoder, and modified inference neural networks, resulting in extensive cross-system redesigns and compatibility issues. This paper proposes a novel communication framework that aligns reconstruction-oriented and task-oriented communications for edge intelligence. The idea is to extend the Information Bottleneck (IB) theory to optimize data transmission by minimizing task-relevant loss function, while maintaining the structure of the original data by an information reshaper. Such an approach integrates task-oriented communications with reconstruction-oriented communications, where a variational approach is designed to handle the intractability of mutual information in high-dimensional neural network features. We also introduce a joint source-channel coding (JSCC) modulation scheme compatible with classical modulation techniques, enabling the deployment of AI technologies within existing digital infrastructures. The proposed framework is particularly effective in edge-based autonomous driving scenarios. Our evaluation in the Car Learning to Act (CARLA) simulator demonstrates that the proposed framework significantly reduces bits per service by 99.19% compared to existing methods, such as JPEG, JPEG2000, and BPG, without compromising the effectiveness of task execution.

**Index Terms**—Task-oriented communication, edge inference, information bottleneck, variational inference.

## I. INTRODUCTION

Reconstruction-oriented communications are designed to recover the transmitted information at the receiver sides, often involving traditional source and channel coding techniques. This approach is commonly used in systems where the fidelity of the information is paramount, such as in audio or video streaming services. The structure of separate source and channel coding, a cornerstone in the design of communication

systems, has been shown to be theoretically optimal via Asymptotic Equipartition Property (AEP) with infinitely long source and channel blocks [1]. However, in practical scenarios, this separation often leads to inefficiencies and suboptimal performance, particularly for Artificial Intelligence (AI) driven applications [2].

The pervasive advancement of AI technologies, particularly in the context of deep learning, presents novel challenges for future communication systems, where the throughput required by AI agents could be much higher than that of human users.

Recent developments in deep learning have shown that Joint Source-Channel Coding (JSCC) can potentially address some of these inefficiencies and outperform traditional separate coding designs. This approach is especially potent in environments where traditional methods struggle to keep pace with the data demands of AI-driven applications. However, JSCC-based reconstruction-oriented communications, which focus on accurately reconstructing a signal on receiver sides, often waste communication resources by transmitting task-agnostic information [3].

To address these issues, task-oriented communication has emerged as a key technology and has attracted significant research interests [4]–[7]. Using the capabilities of deep learning, task-oriented JSCC focuses on transmitting task-specific information, thus improving efficiency and reducing the data rate in critical applications. This requires joint optimization of the JSCC and inference network, which must be co-designed for effective task-oriented communication [4]. Note that existing JSCC designs are mainly based on analog communication principles [2] and cannot be integrated with existing digital communication infrastructures.

Furthermore, cloud-based services introduce unacceptable latency for real-time applications, such as autonomous driving [8], [9]. To mitigate this issue, *edge inference* [4], [10], [11] has become a promising approach, enabling quick response to real-time AI applications. However, widely deployed AI agents bring significant communication loads to communication systems. Emergent methods based on JSCC have shown great potential to solve this problem [11]–[13].

Recognizing these multifaceted challenges, there is a growing interest in developing communication systems that are not only task-oriented but also aligned with reconstruction-oriented communication frameworks. This has led to the proposition of what we refer to as Aligned Task- and Reconstruction-Oriented Communication (ATROC), which aims to bridge the gap between the efficiency of task-specific

Yufeng Diao is with the School of Computing Science, University of Glasgow, UK (e-mail: y.diao.1@research.gla.ac.uk).

Yichi Zhang is with the Department of Computer Science, University of Manchester, UK. Part of this work was done when he was with the James Watt School of Engineering, University of Glasgow, UK (e-mail: yichi.zhang@postgrad.manchester.ac.uk).

Changyang She is with the School of Electrical and Information Engineering, University of Sydney, Australia (e-mail: shechangyang@gmail.com).

Philip Guodong Zhao is with the Department of Computer Science, University of Manchester, UK (e-mail: philip.zhao@manchester.ac.uk).

Emma Liying Li is with the School of Computing Science, University of Glasgow, UK (e-mail: liying.li@glasgow.ac.uk).

data transmission and the robustness of reconstruction-oriented communications, enabling the seamless integration of AI technologies with existing network infrastructures.

### A. Related Works

1) *Joint Source-Channel Coding*: The rapid evolution of deep learning has significantly influenced communication system designs, aiming to achieve or even surpass the Shannon limit. Deep learning based JSCC has emerged as a robust solution in scenarios characterized by limited bandwidth and low Signal-to-Noise Ratio (SNR). Research in deep JSCC for reconstruction-oriented communication [2], [3], [14] has demonstrated its superiority over traditional source coding methods, such as JPEG [15] and JPEG2000 [16], as well as channel coding techniques, such as LDPC codes [17], particularly in environments with low SNR.

Existing reconstruction-oriented communication research primarily focused on data-centric metrics (e.g., Peak Signal-to-Noise Ratio (PSNR) [3], [14], [18]–[20], Structural Similarity (SSIM) [2], [3], [19], [20], and Multi-Scale Structural Similarity (MS-SSIM) [3], [19], [20]) to evaluate the effectiveness of deep JSCC. However, these metrics often lead to suboptimal task performance since high-fidelity reconstructions are not always necessary from the machine’s perspective, whereas task-specific semantic information plays the most important role [21]–[26]. For example, in text transmission, the fidelity of words might be compromised to improve communication efficiency while still conveying the intended meanings [27], [28]. Similarly, in image transmission, image fidelity can be sacrificed for less communication overhead and higher task performance [29]–[31].

Nonetheless, existing works, such as [32], assumed that the amplitudes and phases of channel symbols are analog. Thus, we cannot implement them directly in digital communication systems [33]. To address this issue, the authors of [34] explored image transmission over the discrete channel (binary symmetric channel) using variational learning with a Bernoulli prior. This work was further extended by the authors of [35], who introduced adversarial regularization to enhance robustness. Furthermore, recent works [18], [36] investigated the transmission of natural images over an Additive White Gaussian Noise (AWGN) channel model with a finite channel input alphabet. Despite a good fit between the learned constellation diagram and the latent representation, the irregularity of the constellation diagram still poses significant challenges for deployment on commercial hardware. The author of [37] developed a digital task-oriented communication framework employing a hardware-limited scalar quantization approach, specifically tailored for computation-constrained situations, such as Internet of Things (IoT). The results of this work provide valuable insights for future task-oriented JSCC designs.

2) *Edge Inference*: Edge inference has gained prominence as a solution to meet the stringent latency requirements of modern applications, which are not adequately supported by traditional cloud services [10], [38]. The key architectural approach that underpins recent advancements is *split inference*, where the inference network is partitioned between the device and the edge [4], [5], [11]–[13], [39]–[42].

In this architecture, a mobile device initially processes data using a lightweight neural network to extract a compact feature vector. Subsequently, this vector is transmitted to an edge server for further processing, where deep JSCC is integral to the entire procedure [4], [5], [11]–[13], [42]. Notably, an end-to-end framework that efficiently compresses intermediate features to optimize the bandwidth and computational resources at the edge was introduced in [12]. In addition, the authors of [4] developed a method to flexibly adjust the length of the transmission signal to adapt to dynamic communication environments while maintaining targeted inference accuracy.

Recent studies have shifted from reconstruction-oriented communication, which focuses on accurately reconstructing a signal at the receiver, to a task-oriented approach that prioritizes inference accuracy as the primary performance metric [4], [5], [12], [43], [44]. This paradigm shift underscores a move towards optimizing communication systems to support specific functional requirements rather than general data fidelity.

Note that implementing such split-design architectures often necessitates modifications on both the device and the edge, which pose challenges in terms of compatibility with existing communication infrastructures. This issue highlights a significant barrier to widespread adoption, indicating the need for more compatible solutions that can seamlessly integrate with current technologies.

3) *Variational Information Bottleneck*: The Information Bottleneck (IB) theory, which extends from the foundational rate-distortion theory [1], aims to find an optimal trade-off by maximizing the preservation of task-specific information in the latent representations, while minimizing the inclusion of task-agnostic information from the input data. Initially proposed by [45], the practical application of IB theory in training deep neural networks remained theoretical until significantly later [46].

The application of IB theory in deep learning was primarily hindered by computational challenges. The traditional optimization of the IB objective function relied on the iterative Blahut-Arimoto algorithm [47], [48], which is infeasible for deep learning applications due to its computational complexity and inefficiency in handling large-scale data [46]. Addressing this limitation, [49] introduced a variational approach to construct a tractable lower bound on the IB objective, leading to the development of the Variational Information Bottleneck (VIB) method. This approach enabled the practical application of the IB principles in deep learning by approximating the intractable true posterior with a variational distribution.

Recent work has seen the integration of VIB with deep JSCC, which has been effectively used to formalize task-oriented communication strategies. In particular, the results [4], [5] have demonstrated that combining VIB with deep JSCC offers superior performance over reconstruction-oriented communication frameworks. These studies showcase the potential of VIB in improving the efficiency and robustness of communication systems, particularly in scenarios where preserving task-specific information and discarding task-agnostic information are crucial.

Integrating JSCC and IB methods to protect user privacy is an advanced direction in current research. FedSem [50] had

collaboratively trained semantic-channel encoders of multiple devices coordinated by a semantic-channel decoder using IB theory based on base stations. Unlike traditional centralized learning approaches, FedSem reduces communication overhead and mitigates privacy concerns by enabling the sharing of semantic features rather than raw data. In addition, the author of [51] introduced a privacy-preserving JSCC scheme for image transmission, using a disentangled IB objective to effectively separate private information from public data. This approach ensures the protection of privacy-sensitive information while maintaining high image quality. Although these works show impressive progress in the integration of JSCC with IB theory, they often require specialized designs that are challenging to combine with existing systems and devices.

There is a need to design an advanced framework aligning two communication paradigms – task-oriented communications and reconstruction-oriented communications – and develop a JSCC modulation scheme for practical deployment.

### B. Contributions

This paper introduces a novel communication framework compatible with reconstruction-oriented communication, especially for edge inference, termed Aligned Task- and Reconstruction-Oriented Communication (ATROC). By extending IB theory [45] and incorporating JSCC modulation, this framework is designed to enhance AI-driven applications. It prioritizes task relevance in data transmission strategies, shifting focus from traditional signal reconstruction fidelity to operational efficiency and effectiveness in real-world applications. The key contributions of this research are summarized as follows:

- **Development of an ATROC Framework:** Based on IB theory, we develop a framework that aligns task-oriented communications with reconstruction-oriented communications. The framework focuses on maximizing mutual information between inference results and encoded features, minimizing mutual information between the encoded features and the input data, and preserving task-specific information through the information reshaper. This reshaper is expert at transforming received symbols into task-specific data, maintaining the same data structure as the input while ensuring the preservation of task-specific information.
- **Innovation of an Information Reshaper:** We introduce an information reshaper within our extended IB theory, laying a foundational aspect of ATROC. This component is crucial for adapting the communication to the specific needs of the task without compromising the integrity of the transmitted data.
- **Variational Approximation for Tractable Information Estimation:** Due to the intractability of mutual information in the training and inference of deep neural networks, we employ a variational approximation approach, known as VIB. This approach allows us to establish a tractable upper bound for these terms, enabling training and inference of deep neural networks.
- **Adaptation of a JSCC Modulation Scheme:** We design a JSCC modulation scheme that aligns JSCC symbols

TABLE I  
SUMMARY OF MAIN SYMBOLS

Symbol	Explanation
$x$	Input data
$\hat{x}$	Reconstructed input data
$z$	JSCC symbols
$\tilde{z}$	Quantized JSCC symbols
$z_{\text{in}}$	Channel input
$z_{\text{out}}$	Channel output
$\tilde{\tilde{z}}$	Equalized JSCC symbols
$\tilde{\tilde{\tilde{z}}}$	Scaled JSCC symbols
$\tilde{\tilde{\tilde{\tilde{z}}}}$	Reconstructed JSCC symbols
$y$	Task-specific data
$a$	Target action
$\hat{a}$	Inferred action
$\beta_1, \beta_2, \hat{\beta}_1, \hat{\beta}_2$	Lagrange multiplier
$\phi, \theta, \psi, \delta$	Parameters of neural networks
$h$	Channel coefficient
$n$	Gaussian noise
$k$	Dimension of the JSCC symbols
$l$	Dimension of the input data
$\zeta$	Upper bound of rate
$\Omega$	Size of mini-batch
$u$	Number of constellation points
$r$	Constellation parameter
$e(\cdot)$	Constellation point
$P_{\text{target}}$	Power constraint of transmitter
$P_{\tilde{z}}$	Power of quantized symbols
$\beta_Q$	Hyperparameter of quantization loss
$\Gamma, \lambda_{\text{feat}}, \lambda_{\text{traj}}, \lambda_{\text{ctrl}}, \lambda_{\text{aux}}$	Hyperparameters of edge AI agent
$J_1, J_2$	Sampling number
$i, j$	General index depended on context

with a predefined constellation scheme. This scheme ensures compatibility of our framework with classic modulation techniques, making it more adaptable to existing communication infrastructures.

- **Performance Enhancement in Edge-Based Autonomous Driving:** In our simulation, we validate that the ATROC framework outperforms reconstruction-oriented methods for edge-based autonomous driving [52]. Specifically, our method reduced 99.19% communication load, in terms of bits per service, compared to existing methods, without compromising the driving score of the autonomous driving agent.

### C. Organization and Notations

The rest of this paper is organized as follows: Section II details the system model and discusses how the proposed framework advances reconstruction-oriented and non-aligned task-oriented communication approaches. Section III introduces the IB theory for ATROC and elaborates on the corresponding VIB derivation. In Section IV, we propose a JSCC modulation technique that is compatible with classical modulation methods, such as Quadrature Amplitude Modulation (QAM). Section V extends the framework of VIB to enhance edge-based autonomous driving applications. The experimental results are presented in Section VI, which evaluates the performance of our proposed ATROC framework and the JSCC modulation. Finally, Section VII concludes the paper.

Table I lists the main symbols used throughout this paper.

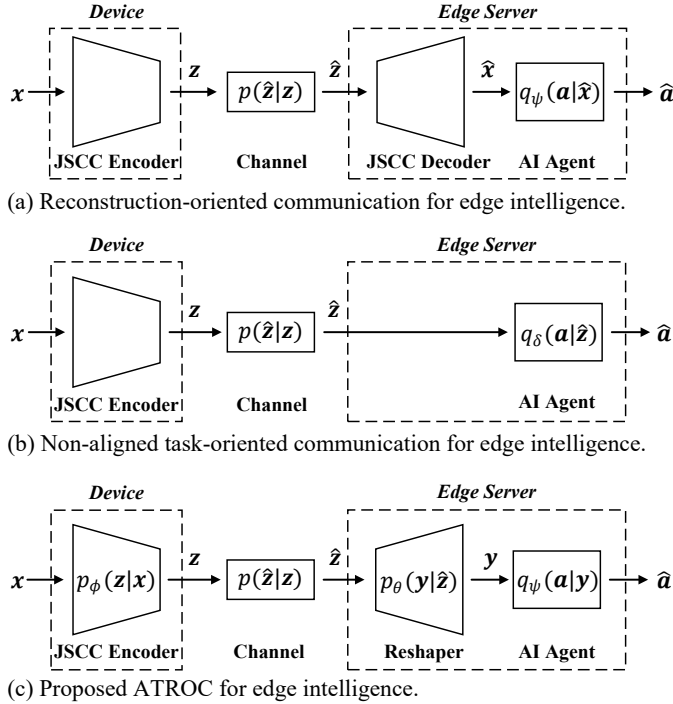


Fig. 1. Comparison of three JSCC-enabled communication frameworks for edge inference: Reconstruction-oriented, non-aligned task-oriented, and ATROC frameworks. All three frameworks can share a similar JSCC encoder structure on the device side. On the edge side, reconstruction-oriented communication aims to fully reconstruct the input data, including both task-specific and task-agnostic information. In contrast, non-aligned task-oriented communication focuses solely on preserving task-specific information and uses JSCC symbols directly for inference. ATROC merges the benefits of the previous two by transferring task-specific information and ensuring that data structures are compatible with existing AI agent networks, enhancing integration and efficiency.

## II. ATROC FRAMEWORK FOR EDGE INTELLIGENCE

Edge intelligence refers to an AI agent (system) that operates at edge servers rather than relying on centralized servers or cloud-based services. These systems process data locally on devices or at the edge of the network as shown in Fig. 1.

The reconstruction-oriented communication framework (see Fig. 1a) aims to preserve all information from the input data  $x$  in the reconstructed data  $\hat{x}$ . The idea is to minimize the distance  $d(x, \hat{x})$ , where  $d(\cdot, \cdot)$  is a predefined data-centric metric. This task-agnostic strategy may result in transmitting redundant data for AI agents, leading to poor resource utilization efficiency.

To improve efficiency, the principle of IB has been developed to transmit task-relevant information [4], as shown in Fig. 1b. However, a significant challenge arises with this approach: the dimensions of the received symbols often do not align with the input dimensions required by the edge AI agent. This mismatch necessitates a redesign of the AI agent to accommodate different input sizes, leading to poor compatibility.

To address this, we propose an ATROC framework, as depicted in Fig. 1c, enabling the use of a unified inference network across both task-oriented and reconstruction-oriented communication paradigms.

In this framework, the JSCC encoder deployed on the mobile device is denoted by  $p_\phi(z|x)$ , where  $\phi$  represents the parameters. The encoder maps the input data  $x \in \mathbb{R}^l$  to JSCC symbols  $z \in \mathbb{C}^k$ , where  $z = [z_1, \dots, z_k]$ . Here,  $l$  and  $k$  are the dimensions of the input data and the JSCC symbols, respectively. After quantization and power normalization, the JSCC symbols  $z$  are transmitted through a physical channel. In this paper, we model the communications between the mobile device and the edge server as Gaussian or Rayleigh fading channels:

$$z_{\text{out}} = h \cdot z_{\text{in}} + \mathbf{n}, \quad (1)$$

where  $z_{\text{in}}$  represents channel input and  $z_{\text{out}}$  represents channel output.  $\mathbf{n} \sim \mathcal{CN}(0, \sigma_n^2 I)$  is a Gaussian noise with zero mean and standard deviation  $\sigma_n$ . For the Gaussian channel, we set  $h = 1$ , whereas for the Rayleigh fading channel,  $h$  is modeled as a complex Gaussian variable,  $h \sim \mathcal{CN}(0, 1)$ , to represent the multipath fading effect.

After the process of equalization, scaling, and detection, the reconstructed symbols  $\hat{z}$  are transformed by the information reshaper  $p_\theta(y|\hat{z})$  with parameters  $\theta$  to provide task-specific data  $y$ . These data are then utilized by the AI agent  $q_\psi(a|y)$  with parameters  $\psi$ , to generate the inferred action  $\hat{a}$ , which approximates the ground truth action  $a$ .

## III. INFORMATION BOTTLENECK FOR ATROC

### A. Problem Description

Following the standard IB framework [45], [49], we assume the joint distribution of the system variables as follows:

$$p(\mathbf{a}, \mathbf{x}, \mathbf{z}, \hat{\mathbf{z}}, \mathbf{y}) = p(\mathbf{a})p(\mathbf{x}|\mathbf{a})p_\phi(\mathbf{z}|\mathbf{x})p(\hat{\mathbf{z}}|\mathbf{z})p_\theta(\mathbf{y}|\hat{\mathbf{z}}). \quad (2)$$

This sets up the Markov chain depicted as:

$$A \leftrightarrow X \leftrightarrow Z \leftrightarrow \hat{Z} \leftrightarrow Y. \quad (3)$$

We introduce a performance metric *bits per service* to measure communication efficiency, which is defined as  $k \cdot c$ , where  $c$  represents bits per symbol. Thus, there exists a crucial trade-off between bits per service and inference accuracy. This relationship underpins the formulation of an IB, where we seek to optimize the balance between information throughput and decision accuracy.

The transformation from reconstructed symbols  $\hat{z}$  to task-specific data  $y$  is designed to preserve task-specific information, aligning task-oriented paradigms with traditional and reconstruction-oriented approaches. Based on the IB theory [45], [49], we formulate the following optimization problem:

$$\min -I(A; Y) \quad (4a)$$

$$\text{s.t. } I(X; \hat{Z}) - \zeta \leq 0, \quad (4b)$$

$$I(A; Y) - I(A; \hat{Z}) = 0, \quad (4c)$$

where  $\zeta$  represents the upper bound of data rate depending on the channel. The data processing inequality [1] implies that, ideally, if  $Y$  and  $\hat{Z}$  contain equivalent information about the action  $A$ , the equality  $I(A; Y) - I(A; \hat{Z}) = 0$  holds.

We further formulate this problem as Eq. (5a), where  $\beta_1 > 0$  and  $\beta_2 > 0$  are the Lagrange multipliers. The detailed deriva-

$$\mathcal{L}_{\text{IB}}(\mathbf{a}, \mathbf{x}; \phi, \theta) = \underbrace{-I(A; Y)}_{\text{Distortion}} + \beta_1 \underbrace{(I(X; \hat{Z}) - \zeta)}_{\text{Rate}} + \beta_2 \underbrace{(I(A; Y) - I(A; \hat{Z}))}_{\text{Alignment}} \quad (5a)$$

$$\equiv -I(A; Y) + \hat{\beta}_1 I(X; \hat{Z}) - \hat{\beta}_2 I(A; \hat{Z}) \quad (5b)$$

$$\equiv \mathbb{E}_{\mathbf{a}, \mathbf{x}} [\mathbb{E}_{\mathbf{y}|\mathbf{x}; \phi, \theta} [-\log p(\mathbf{a}|\mathbf{y})]] + \hat{\beta}_1 D_{\text{KL}}(p_\phi(\hat{\mathbf{z}}|\mathbf{x}) \| p(\hat{\mathbf{z}})) + \hat{\beta}_2 \mathbb{E}_{\mathbf{z}|\mathbf{x}; \phi} [-\log p(\mathbf{a}|\hat{\mathbf{z}})] \quad (5c)$$

tion can be found in Section III-B. The first term  $-I(A; Y)$  and the second term  $I(X; \hat{Z})$  formalize the classic information bottleneck, meanwhile, the third term  $[I(A; Y) - I(A; \hat{Z})]$  aligns the task-relevant information between the task-specific data  $\mathbf{y}$  and the reconstructed symbols  $\hat{\mathbf{z}}$ .

In the case  $\beta_2 \neq 1$ , we define  $\hat{\beta}_1 = \frac{\beta_1}{1-\beta_2}$  and  $\hat{\beta}_2 = \frac{\beta_2}{1-\beta_2}$ . Then Eq. (5a) can be expressed as Eq. (5b). In the case  $\beta_2 = 1$ , Eq. (5a) is simplified to the classic IB formulation [4], [45], [49]:

$$\mathcal{L}_{\text{IB}}(\mathbf{a}, \mathbf{x}; \phi, \theta) = \underbrace{-I(A; \hat{Z})}_{\text{Distortion}} + \beta_1 \underbrace{I(X; \hat{Z})}_{\text{Rate}}. \quad (6)$$

This extended IB theory preserves more task-specific information, and the bits per service is the same as the previous IB approaches. Meanwhile, it maintains the dimension and structure required for edge inference.

### B. Variational Approach

With the objective function Eq. (5b), we first illustrate how to compute each term for training  $\phi$  and  $\theta$ . We start with the first term,  $-I(A; Y)$ , expressed as:

$$\begin{aligned} -I(A; Y) &= -\int p(\mathbf{a}, \mathbf{y}) \log \frac{p(\mathbf{a}|\mathbf{y})}{p(\mathbf{a})} d\mathbf{a} d\mathbf{y} \\ &= -\int p(\mathbf{a}, \mathbf{y}) \log p(\mathbf{a}|\mathbf{y}) d\mathbf{a} d\mathbf{y} - H(A), \end{aligned} \quad (7)$$

where  $p(\mathbf{a}|\mathbf{y})$  is the posterior probability, which can be derived through the Markov Chain [4], [49] as:

$$\begin{aligned} p(\mathbf{a}|\mathbf{y}) &= \int p(\mathbf{a}, \mathbf{x}, \mathbf{z}, \hat{\mathbf{z}}|\mathbf{y}) d\mathbf{x} d\mathbf{z} d\hat{\mathbf{z}} \\ &= \int \frac{p(\mathbf{a})p(\mathbf{x}|\mathbf{a})p_\phi(\mathbf{z}|\mathbf{x})p(\hat{\mathbf{z}}|\mathbf{z})p_\theta(\mathbf{y}|\hat{\mathbf{z}})}{p(\mathbf{y})} d\mathbf{x} d\mathbf{z} d\hat{\mathbf{z}}. \end{aligned} \quad (8)$$

Given the complexity of this integration, we employ a neural network  $q_\psi(\mathbf{a}|\mathbf{y})$  as a variational approximation to  $p(\mathbf{a}|\mathbf{y})$ .

Denoting the Kullback-Leibler (KL) divergence as  $D_{\text{KL}}$ . According to the definition of KL divergence [1], we can derive the following expression:

$$\begin{aligned} D_{\text{KL}}(p(\mathbf{a}|\mathbf{y}) \| q_\psi(\mathbf{a}|\mathbf{y})) &= \int p(\mathbf{a}, \mathbf{y}) \log p(\mathbf{a}|\mathbf{y}) d\mathbf{a} d\mathbf{y} \\ &\quad - \int p(\mathbf{a}, \mathbf{y}) \log q_\psi(\mathbf{a}|\mathbf{y}) d\mathbf{a} d\mathbf{y}. \end{aligned} \quad (9)$$

Based on the fact that

$$D_{\text{KL}}(p(\mathbf{a}|\mathbf{y}) \| q_\psi(\mathbf{a}|\mathbf{y})) \geq 0, \quad (10)$$

we have

$$\begin{aligned} \int p(\mathbf{a}, \mathbf{y}) \log p(\mathbf{a}|\mathbf{y}) d\mathbf{a} d\mathbf{y} \\ \geq \int p(\mathbf{a}, \mathbf{y}) \log q_\psi(\mathbf{a}|\mathbf{y}) d\mathbf{a} d\mathbf{y}, \end{aligned} \quad (11)$$

which derives

$$\begin{aligned} \mathbb{E}_{\mathbf{a}, \mathbf{x}} [\mathbb{E}_{\mathbf{y}|\mathbf{x}; \phi, \theta} [-\log p(\mathbf{a}|\mathbf{y})]] \\ \leq \mathbb{E}_{\mathbf{a}, \mathbf{x}} [\mathbb{E}_{\mathbf{y}|\mathbf{x}; \phi, \theta} [-\log q_\psi(\mathbf{a}|\mathbf{y})]]. \end{aligned} \quad (12)$$

The detailed derivation of Eq. (12) can be found in Appendix A.

The second term  $I(X; \hat{Z})$  [4] is formulated as:

$$I(X; \hat{Z}) = \mathbb{E}_{\mathbf{a}, \mathbf{x}} [D_{\text{KL}}(p_\phi(\hat{\mathbf{z}}|\mathbf{x}) \| p(\hat{\mathbf{z}}))], \quad (13)$$

where the marginal probability is

$$p(\hat{\mathbf{z}}) = \int p(\mathbf{a})p(\mathbf{x}|\mathbf{a})p_\phi(\mathbf{z}|\mathbf{x})p(\hat{\mathbf{z}}|\mathbf{z}) d\mathbf{a} d\mathbf{x} d\mathbf{z}. \quad (14)$$

We adopt a Gaussian approximation  $q(\hat{\mathbf{z}}) \sim \mathcal{N}(\mathbf{0}, I)$  as an estimation for  $p(\hat{\mathbf{z}})$  [53]. It is reasonable as the JSCC encoder generates a Gaussian distribution  $p_\phi(\hat{\mathbf{z}}|\mathbf{x}) \sim \mathcal{N}(\boldsymbol{\mu}_\phi(\mathbf{x}), \boldsymbol{\sigma}_\phi^2(\mathbf{x})I)$ , where  $\boldsymbol{\mu}_\phi(\cdot)$  and  $\boldsymbol{\sigma}_\phi(\cdot)$  are functions that map the input data  $\mathbf{x}$  to the mean and standard deviation of the Gaussian distribution.

Since  $D_{\text{KL}}(p(\hat{\mathbf{z}}) \| q(\hat{\mathbf{z}})) \geq 0$ , the following upper bound can be derived:

$$I(X; \hat{Z}) \leq \mathbb{E}_{\mathbf{a}, \mathbf{x}} [D_{\text{KL}}(p_\phi(\hat{\mathbf{z}}|\mathbf{x}) \| q(\hat{\mathbf{z}}))], \quad (15)$$

where the KL divergence can be calculated analytically by the method in [54].

Similar to Eq. (12), by using  $q_\delta(\mathbf{a}|\hat{\mathbf{z}})$  as a variational approximation of  $p(\mathbf{a}|\hat{\mathbf{z}})$ , we have

$$\begin{aligned} \mathbb{E}_{\mathbf{a}, \mathbf{x}} [\mathbb{E}_{\hat{\mathbf{z}}|\mathbf{x}; \phi, \theta} [-\log p(\mathbf{a}|\hat{\mathbf{z}})]] \\ \leq \mathbb{E}_{\mathbf{a}, \mathbf{x}} [\mathbb{E}_{\hat{\mathbf{z}}|\mathbf{x}; \phi, \theta} [-\log q_\delta(\mathbf{a}|\hat{\mathbf{z}})]]. \end{aligned} \quad (16)$$

The above extended VIB formulation determines the upper bound of the IB objective function (Eq. (5c)), which can be expressed as:

$$\begin{aligned} \mathcal{L}_{\text{VIB}}(\mathbf{a}, \mathbf{x}; \phi, \theta) &= \mathbb{E}_{\mathbf{a}, \mathbf{x}} \left\{ \mathbb{E}_{\mathbf{y}|\mathbf{x}; \phi, \theta} [-\log q_\psi(\mathbf{a}|\mathbf{y})] \right. \\ &\quad + \hat{\beta}_1 D_{\text{KL}}(p_\phi(\hat{\mathbf{z}}|\mathbf{x}) \| q(\hat{\mathbf{z}})) \\ &\quad \left. + \hat{\beta}_2 \mathbb{E}_{\hat{\mathbf{z}}|\mathbf{x}; \phi, \theta} [-\log q_\delta(\mathbf{a}|\hat{\mathbf{z}})] \right\}. \end{aligned} \quad (17)$$

Through Monte Carlo sampling, we train  $\phi$  and  $\theta$  by minimizing this objective function using stochastic gradient descent. Specifically, given a mini-batch of data  $\{(\mathbf{a}_i, \mathbf{x}_i)\}_{i=1}^\Omega$  with batch size  $\Omega$ , if the reconstructed JSCC symbols  $\hat{\mathbf{z}}$  are sampled

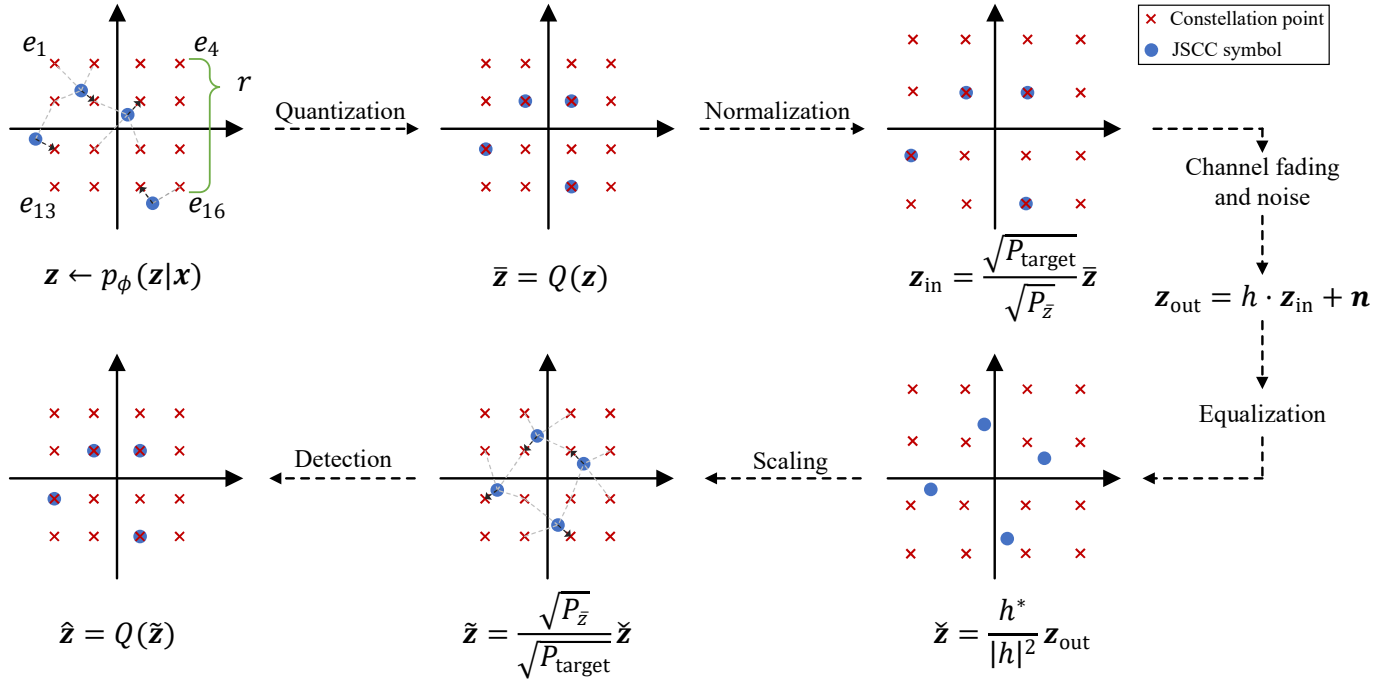


Fig. 2. An example of the JSCC modulation and signal transmission procedure for  $z \in \mathbb{C}^4$  using 16-QAM.

$J_1$  times and the task-specific data  $\mathbf{y}$  are sampled  $J_2$  times for each data pair, the following estimation can be obtained:

$$\mathcal{L}_{\text{VIB}}(\mathbf{a}, \mathbf{x}; \phi, \theta) \cong \frac{1}{\Omega} \sum_{i=1}^{\Omega} \left\{ \frac{1}{J_2} \sum_{j=1}^{J_2} [-\log q_\psi(\mathbf{a}_i | \mathbf{y}_j)] + \hat{\beta}_1 D_{\text{KL}}(p_\phi(\hat{\mathbf{z}} | \mathbf{x}_i) \| q(\hat{\mathbf{z}})) + \frac{\hat{\beta}_2}{J_1} \sum_{j=1}^{J_1} [-\log q_\delta(\mathbf{a}_i | \hat{\mathbf{z}}_j)] \right\}. \quad (18)$$

#### IV. JSCC MODULATION

In existing communication standards, symbols are transmitted with specific constellation orders and designs. In this section, we develop a JSCC modulation scheme that can map arbitrary complex-valued JSCC symbols to a predefined constellation diagram with finite points, as shown in Fig. 2. In addition, we introduce a learning method to adjust the optimal constellation parameter according to the quantization loss. For clarity, we use QAM as an example. Note that our method can be easily extended to other modulation schemes.

##### A. Quantization and Normalization

To enable the quantization of arbitrary complex-valued JSCC symbols into a predefined constellation diagram, the following rule is applied to each symbol:

$$\bar{z}_i = Q(z_i) = \arg \min_{e_j} \|z_i - e_j\|_2^2, \quad (19)$$

where  $z_i \in \mathbb{C}$  represents the original symbol,  $\bar{z}_i \in \mathbb{C}$  represents the quantized symbol,  $i \in \{1, \dots, k\}$ ,  $Q(\cdot)$  denotes the quantization function, and  $\|\cdot\|_2$  denote the  $\ell^2$ -norm.

$e_j \in \{e_1, \dots, e_u\}$  represents the predefined constellation points, where  $e_j \in \mathbb{C}$ , and  $u$  denote the number of constellation points. This quantization operation can be extended to a vector as follows,

$$\bar{\mathbf{z}} = Q(\mathbf{z}) = [Q(z_1), \dots, Q(z_k)]. \quad (20)$$

Since the transmitted symbols should satisfy the average power constraint:

$$\frac{1}{k} \sum_{i=1}^k |\bar{z}_i|^2 \leq P_{\text{target}}, \quad (21)$$

the channel input (normalized symbols) are given by:

$$z_{\text{in}} = \frac{\sqrt{P_{\text{target}}}}{\sqrt{P_{\bar{\mathbf{z}}}}} \bar{\mathbf{z}}, \quad (22)$$

where  $P_{\bar{\mathbf{z}}} = \frac{1}{k} \sum_{i=1}^k |\bar{z}_i|^2$  denotes the power of quantized symbols  $\bar{\mathbf{z}}$ .

The channel input  $z_{\text{in}}$  is transmitted through the channel  $z_{\text{out}} = h \cdot z_{\text{in}} + n$ . Assume that the receiver has the full Channel State Information (CSI) knowledge and knows  $P_{\bar{\mathbf{z}}}$ , in the case of the static channel, it can perform channel equalization:

$$\tilde{\mathbf{z}} = \frac{h^*}{|h|^2} z_{\text{out}}, \quad (23)$$

where  $h^*$  denotes the conjugate of channel coefficient  $h$  and  $\tilde{\mathbf{z}}$  denotes the equalized symbols. After equalization, the equalized symbols should be scaled as

$$\tilde{\tilde{\mathbf{z}}} = \frac{\sqrt{P_{\bar{\mathbf{z}}}}}{\sqrt{P_{\text{target}}}} \tilde{\mathbf{z}}, \quad (24)$$

where  $\tilde{\tilde{\mathbf{z}}}$  denotes the scaled symbols. Then the reconstructed

symbols  $\hat{z} = Q(\tilde{z})$  can be obtained by Eq. (20).

### B. Learnable Constellation Diagram and Fine-Tuning

Traditional modulation techniques, such as QAM, employ a lookup table that maps bits to constellation points. In contrast, the complex-valued channel symbols produced by the JSCC encoder are continuous, necessitating a different approach for their mapping.

Equation (19) demonstrates that the coordinates of each constellation point  $e_j$  directly affect the quantization outcome. We propose a learnable constellation diagram that adapts to the observed space of JSCC symbols, minimizes quantization loss, and improves performance with the JSCC encoder and the information reshaper. Taking  $u$ -QAM as an example, where  $u$  denotes the number of constellation points, the coordinates of each constellation point can be derived by the parameter  $r$ . This parameter specifies the distance between two constellation points located at the corners of one side, as illustrated in Fig. 2. Then, the real part and imaginary part of the constellation point  $e_j$  are given as follows:

$$\text{Re}(e_j) = -\frac{r}{2} + \frac{(j \bmod \sqrt{u}) \cdot r}{\sqrt{u} - 1}, \quad (25)$$

$$\text{Im}(e_j) = \frac{r}{2} - \frac{\lfloor j/\sqrt{u} \rfloor \cdot r}{\sqrt{u} - 1}, \quad (26)$$

where “mod” denotes the modulo operation and  $\lfloor \cdot \rfloor$  denotes the rounding down function.

The quantization loss is defined as

$$\mathcal{L}_Q(\mathbf{z}; r) = \frac{1}{k} \sum_{i=1}^k \min_{e_j} \|z_i - e_j\|_2. \quad (27)$$

The training process for the learnable constellation diagram begins with the initialization of the constellation parameter  $r$  to a predefined value  $r_{\text{init}}$ , along with loading a pre-trained JSCC encoder. Using an image dataset  $\mathcal{X}$  with corresponding ground truth actions  $\mathcal{A}$ , mini-batches are sampled iteratively during training. For each mini-batch, images are encoded into JSCC symbols, and the average batch loss is computed based on the quantization error. The constellation parameter  $r$  is then updated by backpropagation until convergence. The output of this process is the optimal constellation parameter  $r^*$ . The detailed constellation parameter training process is provided in Algorithm 1. Once the optimal  $r^*$  is obtained, the JSCC encoder and the information reshaper are jointly fine-tuned using the extended loss function:

$$\mathcal{L}_{\text{VIB-Q}}(\mathbf{a}, \mathbf{x}; \phi, \theta) = \mathcal{L}_{\text{VIB}}(\mathbf{a}, \mathbf{x}; \phi, \theta) + \beta_Q \mathcal{L}_Q(\mathbf{z}; r^*), \quad (28)$$

where  $\beta_Q$  is a hyperparameter that balances the quantization loss with the original VIB loss.

This method enhances the practical applicability of JSCC modulation by integrating it with established digital communication systems while preserving the benefits of customized encoding and decoding strategies.

---

### Algorithm 1 Training Learnable Constellation Diagram

---

- Initialization:** Initialize the constellation parameter  $r \rightarrow r_{\text{init}}$ , and load pre-trained JSCC encoder  $p_\phi(\mathbf{z}|\mathbf{x})$ .
- 1: **Input:** Image dataset  $\mathcal{X}$  with corresponding ground truth action  $\mathcal{A}$ .
  - 2: **while** not converged **do**
  - 3:   Sample mini-batch  $\{(\mathbf{a}_i, \mathbf{x}_i)\}_{i=1}^\Omega$  from  $\mathcal{X}$  and  $\mathcal{A}$ .
  - 4:   Encode image  $\{\mathbf{x}_i\}_{i=1}^\Omega$  to symbols  $\{\mathbf{z}_i\}_{i=1}^\Omega$ .
  - 5:   Compute the average batch loss  $\frac{1}{\Omega} \sum_{i=1}^\Omega \mathcal{L}_Q(\mathbf{z}_i; r)$ .
  - 6:   Update parameter  $r$  through backpropagation.
  - 7: **end while**
  - 8: **Output:** Optimal constellation parameter  $r^*$ .
- 

## V. EXTENDED VIB FOR EDGE-BASED AUTONOMOUS DRIVING

Trajectory-Guided Control Prediction (TGCP)<sup>1</sup> is the state-of-the-art End-to-End (E2E) self-driving framework that combines trajectory planning and multi-stage control prediction into a unified neural network [52]. This framework, notable for using only a monocular camera, ranks third on the CARLA leaderboard<sup>2</sup>. We extend VIB to TGCP to examine its applicability in an edge-based autonomous driving system.

### A. Background of TGCP

TGCP at the edge server processes task-specific data  $\mathbf{y}$  and additional state information  $\mathbf{m}$  to make driving decisions. The state information includes variables such as speed, destination coordinates, and current driving guidance (e.g., “turn left” or “follow the lane”). For this study, we assume that  $\mathbf{m}$  can be transmitted losslessly to the edge server.

The autonomous driving agent is modeled as  $q_\psi(\mathbf{a}|\mathbf{y})$ , which generates the inferred action  $\hat{\mathbf{a}}$  from task-specific data  $\mathbf{y}$ . In particular, the individual components of the inferred action  $\hat{\mathbf{a}} = (\hat{v}, \hat{s}, \hat{w}, \hat{\mathbf{f}}^{\text{traj}}, \hat{\mathbf{b}}, \hat{\mathbf{f}}^{\text{ctrl}})$  are defined as follows:

- $\hat{v}$ : estimated target speed.
- $\hat{s}$ : value of the extracted features estimated by the expert [55].
- $\hat{w}$ : predicted waypoints from the trajectory branch.
- $\hat{\mathbf{f}}^{\text{traj}}$ : estimated extracted features for trajectory planning.
- $\hat{\mathbf{b}} = [\hat{\mathbf{b}}_0, \hat{\mathbf{b}}_1, \dots, \hat{\mathbf{b}}_\Gamma]$ : estimated control actions from the beta distribution in the control prediction branch, where  $\Gamma$  denotes the prediction length.
- $\hat{\mathbf{f}}^{\text{ctrl}} = [\hat{\mathbf{f}}_0^{\text{ctrl}}, \hat{\mathbf{f}}_1^{\text{ctrl}}, \dots, \hat{\mathbf{f}}_\Gamma^{\text{ctrl}}]$ : predicted informative features of the control prediction branch.

### B. Control and Trajectory Prediction Loss Functions

The designed controller, based on [52], computes control commands such as throttle, steer, and brake using the output

<sup>1</sup>To avoid confusion with the Transmission Control Protocol (TCP), we denote Trajectory-guided Control Prediction as TGCP in this paper.

<sup>2</sup> <https://leaderboard.carla.org/leaderboard/>

of the trajectory and control prediction branches. The corresponding loss functions are defined as:

$$\mathcal{L}_{\text{traj}} = \|\mathbf{w} - \hat{\mathbf{w}}\|_1 + \lambda_{\text{feat}} \|\mathbf{f}^{\text{traj}} - \hat{\mathbf{f}}^{\text{traj}}\|_2, \quad (29)$$

$$\begin{aligned} \mathcal{L}_{\text{ctrl}} = & D_{\text{KL}}(\mathcal{B}e(\mathbf{b}_0) \| \mathcal{B}e(\hat{\mathbf{b}}_0)) \\ & + \frac{1}{\Gamma} \sum_{i=1}^{\Gamma} D_{\text{KL}}(\mathcal{B}e(\mathbf{b}_i) \| \mathcal{B}e(\hat{\mathbf{b}}_i)) \\ & + \lambda_{\text{feat}} \|\mathbf{f}_0^{\text{ctrl}} - \hat{\mathbf{f}}_0^{\text{ctrl}}\|_2 + \frac{1}{\Gamma} \sum_{i=1}^{\Gamma} \|\mathbf{f}_i^{\text{ctrl}} - \hat{\mathbf{f}}_i^{\text{ctrl}}\|_2, \quad (30) \end{aligned}$$

where  $\lambda_{\text{feat}}$  is a hyperparameter,  $\mathbf{w}$ ,  $\mathbf{f}^{\text{traj}}$ ,  $\mathbf{b}_i$ , and  $\mathbf{f}_i^{\text{ctrl}}$  are from the ground truth action  $\mathbf{a}$ ,  $\|\cdot\|_1$  denotes the  $\ell_1$ -norm, and  $\mathcal{B}e(\cdot)$  denotes the beta distribution.

Furthermore, the auxiliary loss function is defined as:

$$\mathcal{L}_{\text{aux}} = \|v - \hat{v}\|_1 + \|s - \hat{s}\|_2, \quad (31)$$

where speed  $v$  and value of features  $s$  are from the ground truth action  $\mathbf{a}$ . Combining these terms, the overall loss function  $\mathcal{L}_{\text{TCGP}}$  becomes:

$$\mathcal{L}_{\text{TCGP}} = \lambda_{\text{traj}} \mathcal{L}_{\text{traj}} + \lambda_{\text{ctrl}} \mathcal{L}_{\text{ctrl}} + \lambda_{\text{aux}} \mathcal{L}_{\text{aux}}, \quad (32)$$

where  $\lambda_{\text{traj}}$ ,  $\lambda_{\text{ctrl}}$ , and  $\lambda_{\text{aux}}$  are hyperparameters.

### C. Task-Oriented End-to-End Training

Typically, we assume that the posterior  $q_{\psi}(\mathbf{a}|\mathbf{y})$  follows a Gaussian distribution  $\mathcal{N}(\boldsymbol{\mu}_{\psi}(\mathbf{y}), \boldsymbol{\Sigma}_{\psi}(\mathbf{y}))$ , where  $\boldsymbol{\mu}_{\psi}(\mathbf{y}) \in \mathbb{R}^d$  and  $\boldsymbol{\Sigma}_{\psi}(\mathbf{y}) = \sigma_c^2 I_d$  ( $\sigma_c$  is a constant). According to the probability density function of the Gaussian distribution, we can derive the following expression,

$$-\log q_{\psi}(\mathbf{a}|\mathbf{y}) \sim \frac{1}{2\sigma_c^2} \|\mathbf{a} - \boldsymbol{\mu}_{\psi}(\mathbf{y})\|_2^2, \quad (33)$$

where  $\boldsymbol{\mu}_{\psi}(\mathbf{y}) = \hat{\mathbf{a}}$ . Details of the derivation are deferred to the Appendix B. Eq. (33) shows that  $-\log q_{\psi}(\mathbf{a}|\mathbf{y})$  can serve as a distance metric, like the  $\ell^2$ -norm. Since  $\mathcal{L}_{\text{TCGP}}$  is a combination of distance metric of action  $\mathbf{a}$  ( $\ell^1$ -norm,  $\ell^2$ -norm, and KL divergence), we heuristically propose substituting the first term in Eq. (17) with  $\mathcal{L}_{\text{TCGP}}$  to adapt the objective function as:

$$\begin{aligned} \mathcal{L}'_{\text{VIB}}(\mathbf{a}, \mathbf{x}; \phi, \theta) = & \mathbb{E}_{\mathbf{a}, \mathbf{x}} \left\{ \mathcal{L}_{\text{TCGP}} \right. \\ & + \hat{\beta}_1 D_{\text{KL}}(p_{\phi}(\hat{\mathbf{z}}|\mathbf{x}) \| q(\hat{\mathbf{z}})) \\ & \left. + \hat{\beta}_2 \mathbb{E}_{\hat{\mathbf{z}}|\mathbf{x}; \phi, \theta} [-\log q_{\delta}(\mathbf{a}|\hat{\mathbf{z}})] \right\}. \quad (34) \end{aligned}$$

In addition, the Eq. (28) can be modified as:

$$\mathcal{L}'_{\text{VIB-Q}}(\mathbf{a}, \mathbf{x}; \phi, \theta) = \mathcal{L}'_{\text{VIB}}(\mathbf{a}, \mathbf{x}; \phi, \theta) + \beta_Q \mathcal{L}_Q(\mathbf{z}; r^*). \quad (35)$$

Training of JSCC encoder and information resaper consists of two stages: pre-training and fine-tuning. In pre-training, the neural network parameters ( $\phi$  and  $\theta$ ) are initialized, and images from the dataset are encoded into JSCC symbols, transmitted through a channel without modulation, and reshaped into task-specific data. The TGCP model, with frozen parameters, generates inferred actions  $\hat{\mathbf{a}}$ , and the loss  $\mathcal{L}'_{\text{VIB}}$  is computed to update the network parameters. Fine-tuning follows a similar process, but the symbols are transmitted

### Algorithm 2 Training JSCC Encoder and Information Resaper.

---

**Initialization:** Initialize the neural network parameters  $\phi$  and  $\theta$ .

- 1: **Input:** Image dataset  $\mathcal{X}$  with corresponding ground-truth agent output  $\mathcal{A}$ . Well-trained TGCP model with frozen parameters. Learning rate  $\eta$ .
- 2: **while** not converged **do**
- 3:   Sample mini-batch  $\{(\mathbf{a}_i, \mathbf{x}_i)\}_{i=1}^{\Omega}$  from  $\mathcal{A}$  and  $\mathcal{X}$ .
- 4:   **for** sample  $i = 1, \dots, \Omega$  **do**
- 5:     Encode image  $\mathbf{x}_i$  to JSCC symbols  $\mathbf{z}_i$ .
- 6:     Transmit JSCC symbols through a channel without JSCC modulation:  $\hat{\mathbf{z}}_i \leftarrow \text{CH}(\mathbf{z}_i)$ .
- 7:     Reshape the reconstructed JSCC symbols  $\hat{\mathbf{z}}_i$  to task-specific data  $\mathbf{y}_i$ .
- 8:     Generate inferred action:  $\hat{\mathbf{a}}_i \leftarrow \text{TGCP}(\mathbf{y}_i)$ .
- 9:     Compute loss  $\mathcal{L}'_{\text{VIB}}$  based on Eq. (34).
- 10:   **end for**
- 11:   Update parameters (pre-training):  
 $\phi \leftarrow -\eta \cdot \nabla_{\phi} \mathcal{L}'_{\text{VIB}}, \theta \leftarrow -\eta \cdot \nabla_{\theta} \mathcal{L}'_{\text{VIB}}$ .
- 12: **end while**
- 13: Find optimal constellation parameter  $r^*$  according to Algorithm 1.
- 14: **while** not converged **do**
- 15:   Sample mini-batch  $\{(\mathbf{a}_i, \mathbf{x}_i)\}_{i=1}^{\Omega}$  from  $\mathcal{A}$  and  $\mathcal{X}$ .
- 16:   **for** sample  $i = 1, \dots, \Omega$  **do**
- 17:     Encode image  $\mathbf{x}_i$  to JSCC symbols  $\mathbf{z}_i$ .
- 18:     Transmit JSCC symbols through a channel with JSCC modulation:  $\hat{\mathbf{z}}_i \leftarrow \text{CH}(\mathbf{z}_i)$ .
- 19:     Reshape the reconstructed JSCC symbols  $\hat{\mathbf{z}}_i$  to task-specific data  $\mathbf{y}_i$ .
- 20:     Generate inferred action:  $\hat{\mathbf{a}}_i \leftarrow \text{TGCP}(\mathbf{y}_i)$ .
- 21:     Compute loss  $\mathcal{L}'_{\text{VIB-Q}}$  based on Eq. (35).
- 22:   **end for**
- 23:   Update parameters (fine-tuning):  
 $\phi \leftarrow -\eta \cdot \nabla_{\phi} \mathcal{L}'_{\text{VIB-Q}}, \theta \leftarrow -\eta \cdot \nabla_{\theta} \mathcal{L}'_{\text{VIB-Q}}$ .
- 24: **end while**
- 25: **Output:** Neural network parameters:  $\phi$  and  $\theta$ .

---

with JSCC modulation, and the loss  $\mathcal{L}'_{\text{VIB-Q}}$  is used for parameter updates. Finally, the optimized parameters  $\phi$  and  $\theta$  are output. The training process of the proposed aligned task- and reconstruction-oriented JSCC encoder and information resaper is shown in Algorithm 2. Here,  $\text{CH}(\cdot)$  denotes the function of a JSCC modulation and communication channel, while  $\text{TGCP}(\cdot)$  denotes the function of TGCP. Specifically, during the fine-tuning process, both the JSCC encoder and the information resaper are actively adjusted, which means that neither component is frozen. This fine-tuning process reduces the quantization loss of the encoder's output and preserves task-critical information, showing the potential for real-world applications.



## VI. PERFORMANCE EVALUATION

### A. Experiment Setup

1) *Dataset*: We utilize the Car Learning to Act (CARLA) simulator, an open-source platform designed for autonomous driving research [56], which provides a variety of urban environments that simulate real-world traffic scenarios. The image dataset from [52], comprising images from various urban maps, serves as the input data  $\mathbf{x}$  for our training. In our experiments, the training dataset consists of 189,524 images from four maps: Town01, Town03, Town04, and Town06. The test dataset includes 27,201 images from another four maps: Town02, Town05, Town07, and Town10.

2) *Evaluation Metrics*: Our evaluation focuses on comparing the driving performance of our ATROC framework against various baselines within the CARLA simulator. We use the commonly adopted driving score<sup>3</sup> to assess the vehicle's ability to navigate according to predetermined waypoints, destinations, and comply with traffic regulations. Each test is conducted three times in Town05 under four different weather scenarios: clear noon, cloudy sunset, soft rain at dawn, and hard rain at night.

3) *Basic Settings*: In our proposed framework, we configure the JSCC symbols dimension  $k$  to 1024, enabling us to achieve significantly low bits per service of 6144 for 64-QAM. For training of the JSCC encoder and the information resaper, we set the Lagrange multipliers  $\hat{\beta}_1 = 1$ ,  $\hat{\beta}_2 = 8192$ , and the quantization loss hyperparameter  $\beta_Q = 10$ , which is a good balance between fidelity and compression. Furthermore, we set the learning rate  $\eta$  to  $4 \times 10^{-5}$ , and impose a power constraint with  $P_{\text{target}} = 1$ .

The TGCP model is trained following the instructions of [52]. In addition, the pre-trained parameters  $\psi$  of TGCP are kept fixed throughout all training phases. This pre-trained TGCP model serves as the AI agent in the following experiments.

For simplicity, a deterministic information resaper is used, allowing us to approximate  $q_\delta(\mathbf{a}|\hat{\mathbf{z}})$  by  $q_\psi(\mathbf{a}|\mathbf{y})$ . The architecture and detailed parameters of the proposed JSCC encoder and the information resaper are shown in Fig. 3.

4) *Baseline Methods*: Three traditional image coding methods are included as baseline methods for comparison: (1) JPEG [15]; (2) JPEG2000 [16]; (3) and BPG [57]. Each traditional image coding method is followed by (2048, 6144) Low-Density Parity-Check (LDPC) codes combined with a 64-QAM digital modulation scheme. The average bits per service for these methods range from 36,844 to 1,041,758.

In addition, baseline methods also include two state-of-the-art reconstruction-oriented JSCC designs, with the legends "ROC-AE" [2] and "ROC-VAE" [58], which represent traditional autoencoder and variational autoencoder approaches. Note that the training dataset for the ROC-AE, ROC-VAE, ATROC, and pre-trained TGCP is identical. For a fair comparison, ROC-AE, ROC-VAE, and ATROC use the same network structure, resulting in the same bits per service (i.e., 6144). In particular, ROC-VAE and ROC-AE are also fine-tuned by our proposed JSCC modulation scheme for 64-QAM,

where the optimal constellation parameters  $r^*$  are 4 and 50.4, respectively.

### B. Results of JSCC Modulation

The constellation parameter  $r$  is trained using a pre-trained JSCC encoder, as described in Algorithm 1. Figure 4 demonstrates that regardless of the initial value of the constellation parameter,  $r_{\text{init}} \in \{1, \dots, 10\}$ , the optimal constellation parameter  $r^*$  consistently converges, validating the effectiveness of the proposed modulation approach.

Driving scores from different fine-tuned models across various constellation parameters based on 64-QAM are presented in Fig. 5. The model fine-tuned with the optimal constellation parameter  $r^*$  outperforms other models under the AWGN channel with SNRs range from -10 dB to 10 dB, showcasing the superiority of our proposed JSCC modulation scheme.

### C. Evaluation on CARLA

The impact of bits per service on the driving score is illustrated in Fig. 6, where the driving score of TGCP using raw images without communication is 25.34. Notably, our proposed method achieves significant bandwidth savings (99.19% compared to existing methods) while maintaining a required driving score of 20 under both the AWGN and Rayleigh fading channels. This substantial reduction in bits per service not only illustrates the efficiency of our approach but also underscores its capability to operate effectively under stringent bandwidth constraints.

Detailed results for specific channel conditions are shown in Fig. 7a and Fig. 7b, demonstrating the dependency of driving scores on SNR. For traditional image coding methods, such as JPEG, JPEG2000, and BPG, we apply two configurations for comparison: (1) the average bits per service are set to 961,484 for JPEG\*, 1,041,758 for JPEG2000\*, and 759,683 for BPG\*; (2) the average bits per service are reduced to 524,996 for JPEG<sup>-</sup>, 472,958 for JPEG2000<sup>-</sup>, and 442,152 for BPG<sup>-</sup>. The first configuration highlights the optimal performance of traditional image coding methods, as shown in Fig. 6a and Fig. 6b. In contrast, the second configuration approximately halves the bits per service from the first, as a basis for further comparison. In contrast, our method requires only 6144 bits per service, highlighting its superior compression and transmission efficiency. In addition, we compare the proposed method ATROC with the state-of-the-art reconstruction-oriented JSCC designs using the same neural network structure, with the legends "ROC-AE" [2] and "ROC-VAE" [58].

Under AWGN channel conditions, our method significantly outperforms reconstruction-oriented communication methods with driving scores of 15.72 at SNR = 0 dB, 15.18 at SNR = -5 dB, and 10.67 at SNR = -10 dB, as shown in Fig. 7a. Traditional methods (JPEG\*, JPEG<sup>-</sup>, JPEG2000\*, JPEG2000<sup>-</sup>, BPG\*, and BPG<sup>-</sup>.) show a dramatic decline in the driving score as SNR decreases (below 0 dB), emphasizing the robustness of our ATROC framework under challenging conditions.

<sup>3</sup> <https://leaderboard.carla.org/>

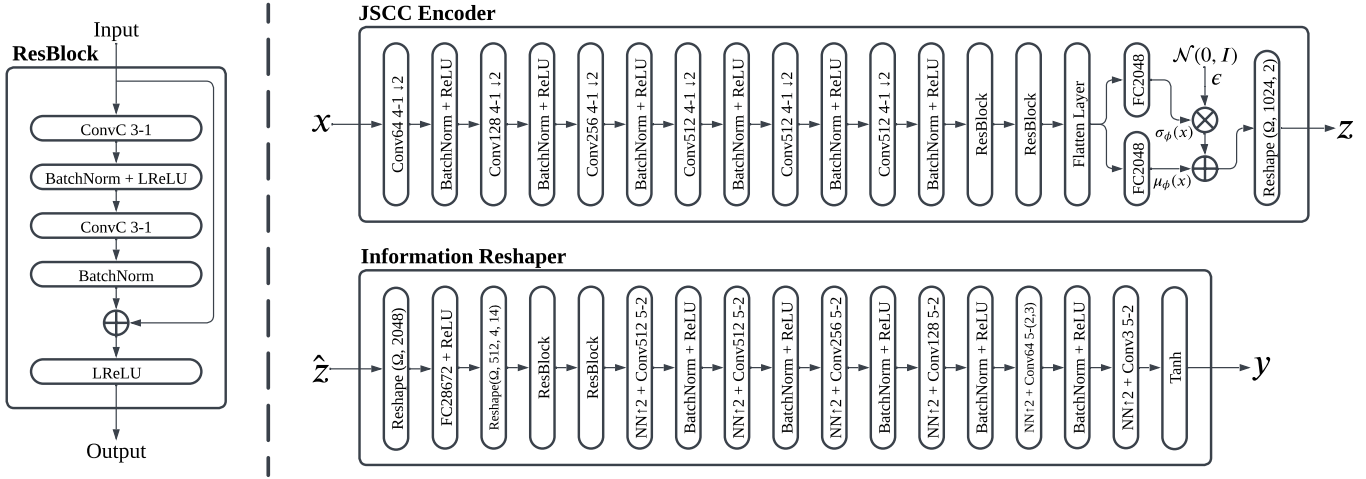


Fig. 3. Architecture of the proposed JSCC encoder and information reshaper. For example, *ConvC 3-1* represents a convolutional layer with  $C$  channels, a  $3 \times 3$  kernel size, and padding of 1 on both sides.  $\downarrow 2$  denotes the strided down convolutions, while  $\text{NN}\uparrow 2$  denotes the nearest neighbor upsampling. *FC2048* refers to a fully connected layer with an output size of 2048. *BatchNorm* denotes batch normalization, *LReLU* represents the leaky ReLU activation with  $\alpha = 0.2$ , and  $\Omega$  represents the batch size. The dimensions (number of channels) of the inputs and outputs for the *ResBlock* remain unchanged.

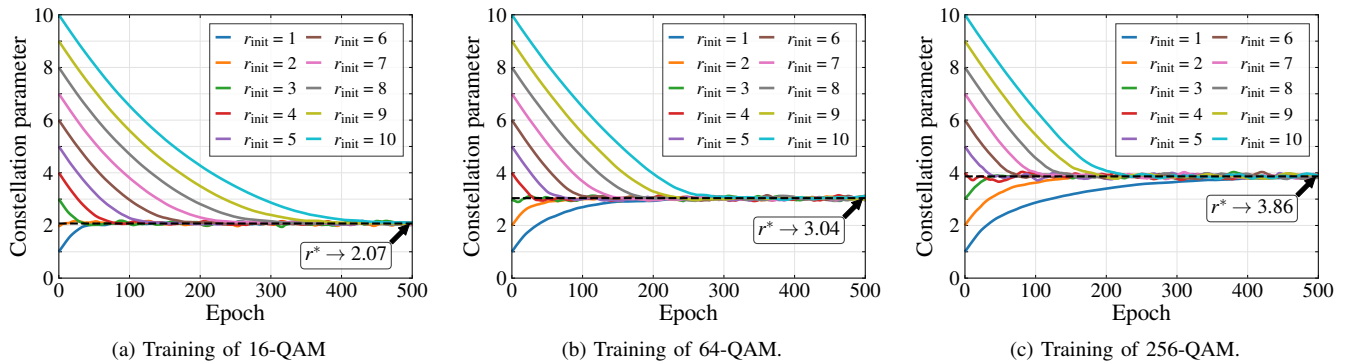


Fig. 4. Training of the constellation parameter for 16-QAM, 64-QAM, and 256-QAM. Regardless of the initial value of the constellation parameter, the optimal value consistently converges.

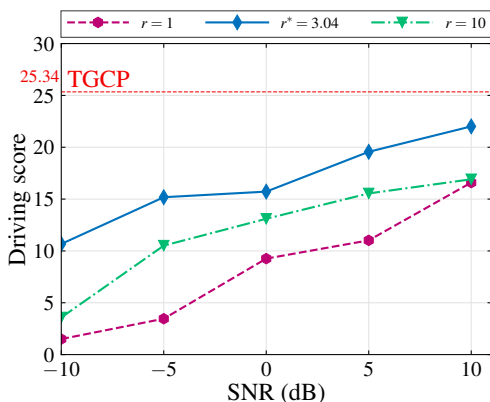


Fig. 5. Driving score of fine-tuned models based on 64-QAM with different constellation parameters ( $r \in \{1, r^*, 10\}$ , where  $r^* = 3.04$ ) under the AWGN channel with SNR range from -10 dB to 10 dB.

Similarly, in Rayleigh fading channel scenarios (Fig. 7b), our proposed method continues to demonstrate superior per-

formance with driving scores of 18.57 at SNR = 10 dB, 13.1 at SNR = 5 dB, and 12.73 at SNR = 0 dB. However, traditional methods experience significant performance degradation when SNR is below 10 dB.

Moreover, JSCC-based reconstruction-oriented communication methods perform poorly under this extremely limited communication bandwidth, as these methods fail to preserve task-specific information.

These findings are further supported by qualitative analysis, as illustrated in Fig. 8. JSCC-based reconstruction-oriented communication methods, while capable of producing high-quality image reconstructions suitable for human vision, often fail to retain crucial task-specific information, such as vehicles, cyclists, road markers, and traffic lights. This deficiency leads to poor performance in edge-based autonomous driving applications, where precise detection of such elements is critical for safety and efficiency. In contrast, our proposed method can effectively preserve task-specific information, shown in the blue, red, and purple boxes of Fig. 8. To reduce the required bits per service, it ignores task-agnostic information, shown in the green box of Fig. 8. Moreover, our proposed method

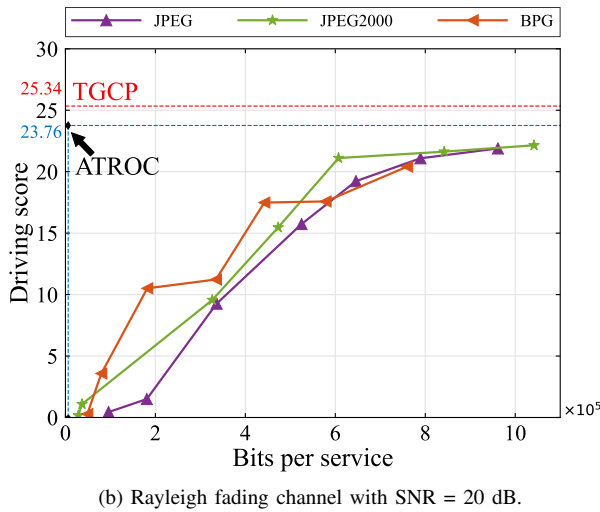
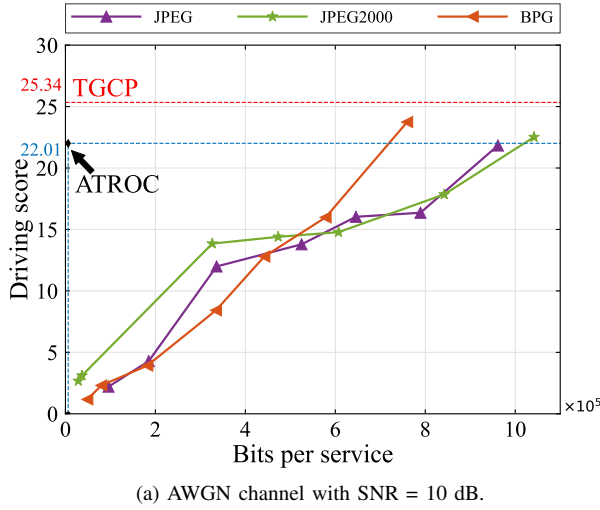


Fig. 6. Driving score of traditional reconstruction-oriented communication with varied bits per service under AWGN channel and Rayleigh channel. The ATROC with 6144 bits per service serves as a baseline for comparison across both channel conditions. In addition, the TCGP using raw RGB images ( $5.5296 \times 10^6$  bits per service) for autonomous driving is also included as a baseline.

demonstrates remarkable noise resistance under low SNR conditions. It effectively preserves task-specific information, maintaining its completeness even in challenging communication environments.

Furthermore, in Table II, we evaluate additional performance metrics such as PSNR, MS-SSIM, and Fréchet Inception Distance (FID), which are typically used to assess image quality from a human perspective. The divergence in performance metrics between traditional reconstruction-oriented methods and our proposed method highlights the necessity of a communication design that prioritizes machine vision, particularly in applications where decision-making accuracy is critical.

## VII. CONCLUSION

This paper has investigated an ATROC framework for edge intelligence, aimed at improving the integration of AI technologies within existing communication infrastructures. By ex-

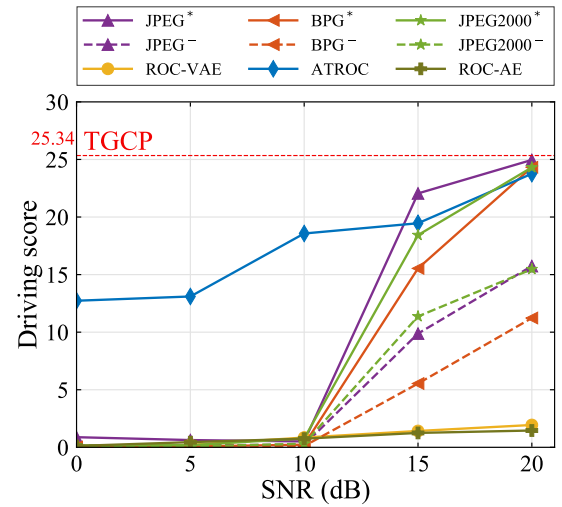
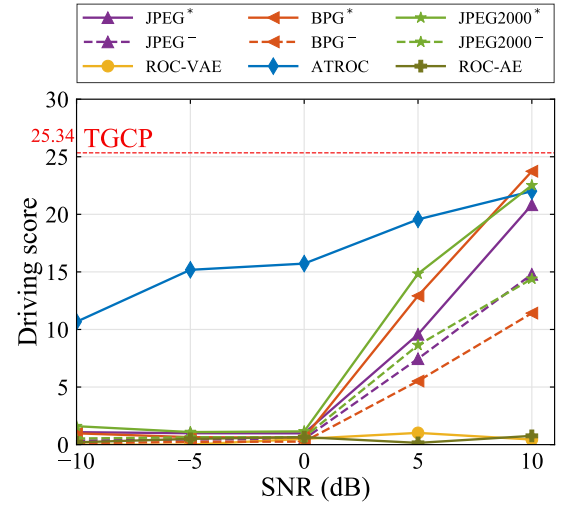


Fig. 7. Driving score with varied SNRs under AWGN channel and Rayleigh channel.

TABLE II  
HUMAN PERCEPTUAL METRICS

Method	$k \cdot c$	PSNR(dB) $\uparrow$	MS-SSIM $\uparrow$	FID $\downarrow$
JPEG	961484	34.56	0.99	5.83
JPEG2000	1041758	37.54	0.99	7.17
BPG	759683	34.93	0.98	6.68
ROC-AE	6144	17.24	0.41	200.59
ROC-VAE	6144	21.75	0.72	135.68
TOC	6144	11.43	0.27	268.14

tending the IB theory and incorporating JSCC modulation, our framework shifts the focus from traditional signal reconstruction fidelity to task relevance, thus optimizing the performance of AI-driven applications in bandwidth-constrained and noise-interference environments.

Our evaluations conducted within the CARLA simulator highlight the robustness of the proposed ATROC framework. Particularly in low SNR conditions, our framework demonstrated significant superiority over traditional reconstruction-

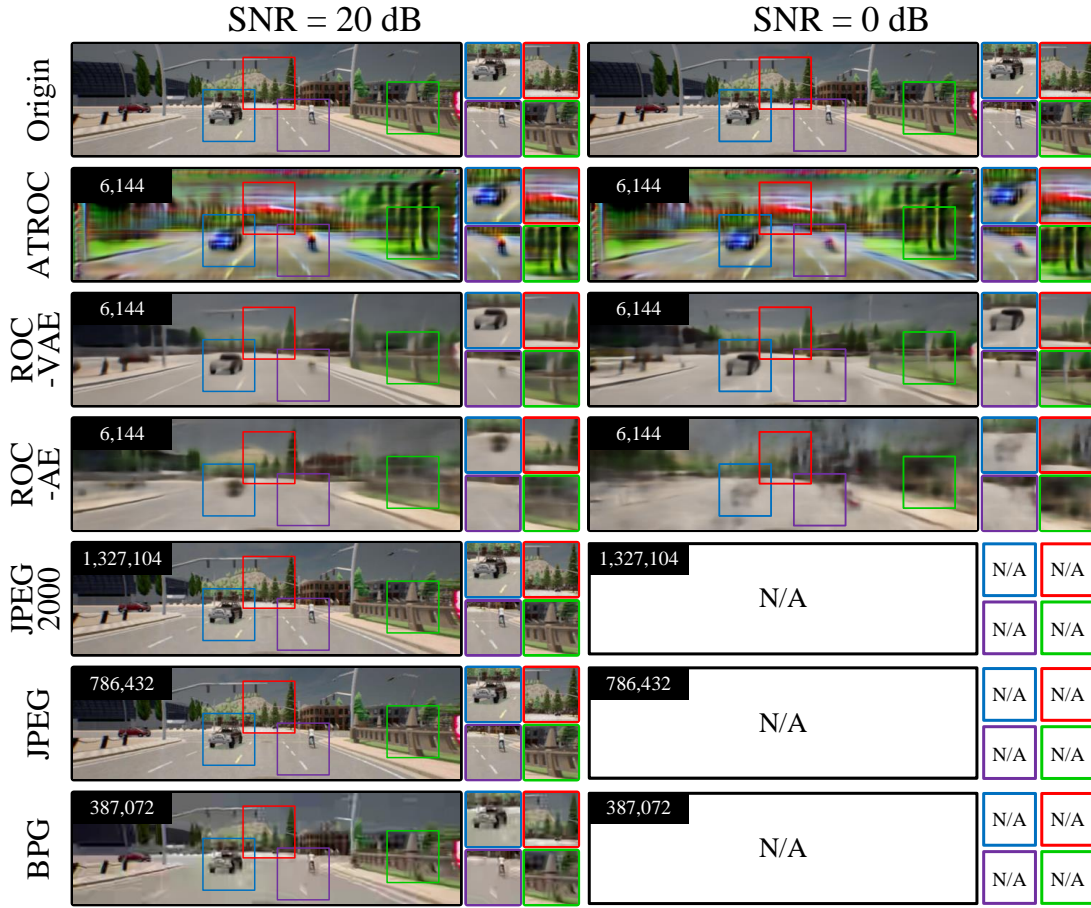


Fig. 8. A qualitative example of our proposed method and baseline methods under Rayleigh fading channel with SNR = 20 dB and SNR = 0 dB. The bits per service of each image are provided in the upper left corner. The details in the reconstructed image are highlighted on the right side of the image. 1) blue box: vehicle and road marks; 2) red box: traffic lights; 3) purple box: cyclist and road marks; 4) green box: fence in the distance. Since traditional reconstruction-oriented communication methods (JPEG, JPEG2000, and BPG) fail to reconstruct images when SNR = 0 dB, we use “N/A” (Not Applicable) to represent the corrupted images.

oriented communication methods by achieving a reduction of up to 99.19% bits per service without sacrificing the effectiveness of task execution.

The qualitative analysis revealed that while reconstruction-oriented communication methods are effective for human visual perception, they often fail to satisfy the specific requirements of machine vision. This observation emphasizes the need for communication designs that align more closely with the specific information needs of AI systems rather than human interpretation.

#### APPENDIX A DERIVATION OF (12)

According to the left part of Eq. (11), we can obtain

$$\begin{aligned}
 & \int p(\mathbf{a}, \mathbf{y}) \log p(\mathbf{a}|\mathbf{y}) \, d\mathbf{a} \, d\mathbf{y} \\
 &= \int p(\mathbf{a}, \mathbf{x}, \mathbf{z}, \hat{\mathbf{z}}, \mathbf{y}) \log p(\mathbf{a}|\mathbf{y}) \, d\mathbf{a} \, d\mathbf{x} \, d\mathbf{z} \, d\hat{\mathbf{z}} \, d\mathbf{y} \\
 &= \int p(\mathbf{a}, \mathbf{x}) p(\mathbf{z}, \hat{\mathbf{z}}, \mathbf{y}|\mathbf{a}, \mathbf{x}) \log p(\mathbf{a}|\mathbf{y}) \, d\mathbf{a} \, d\mathbf{x} \, d\mathbf{z} \, d\hat{\mathbf{z}} \, d\mathbf{y}
 \end{aligned}$$

Considering the Markov chain  $A \rightarrow X \rightarrow Z \rightarrow \hat{Z} \rightarrow Y$ , we have  $p(\mathbf{z}, \hat{\mathbf{z}}, \mathbf{y}|\mathbf{a}, \mathbf{x}) = p(\mathbf{z}, \hat{\mathbf{z}}, \mathbf{y}|\mathbf{x})$ . Since  $\int p(\mathbf{z}, \hat{\mathbf{z}}, \mathbf{y}|\mathbf{x}) \, d\mathbf{z} \, d\hat{\mathbf{z}} = p(\mathbf{y}|\mathbf{x})$ , we can obtain

$$\begin{aligned}
 & \int p(\mathbf{a}, \mathbf{x}) p(\mathbf{z}, \hat{\mathbf{z}}, \mathbf{y}|\mathbf{a}, \mathbf{x}) \log p(\mathbf{a}|\mathbf{y}) \, d\mathbf{a} \, d\mathbf{x} \, d\mathbf{z} \, d\hat{\mathbf{z}} \, d\mathbf{y} \\
 &= \int p(\mathbf{a}, \mathbf{x}) p(\mathbf{y}|\mathbf{x}) \log p(\mathbf{a}|\mathbf{y}) \, d\mathbf{a} \, d\mathbf{x} \, d\mathbf{y} \\
 &= \mathbb{E}_{\mathbf{a}, \mathbf{x}} [\mathbb{E}_{\mathbf{y}|\mathbf{x}; \phi, \theta} [\log p(\mathbf{a}|\mathbf{y})]].
 \end{aligned}$$

Similarly, we can obtain

$$\int p(\mathbf{a}, \mathbf{y}) \log q_{\psi}(\mathbf{a}|\mathbf{y}) \, d\mathbf{a} \, d\mathbf{y} = \mathbb{E}_{\mathbf{a}, \mathbf{x}} [\mathbb{E}_{\mathbf{y}|\mathbf{x}; \phi, \theta} [\log q_{\psi}(\mathbf{a}|\mathbf{y})]].$$

Based on Eq. (11), we can obtain

$$\mathbb{E}_{\mathbf{a}, \mathbf{x}} [\mathbb{E}_{\mathbf{y}|\mathbf{x}; \phi, \theta} [\log p(\mathbf{a}|\mathbf{y})]] \geq \mathbb{E}_{\mathbf{a}, \mathbf{x}} [\mathbb{E}_{\mathbf{y}|\mathbf{x}; \phi, \theta} [\log q_{\psi}(\mathbf{a}|\mathbf{y})]],$$

so that

$$\begin{aligned}
 & \mathbb{E}_{\mathbf{a}, \mathbf{x}} [\mathbb{E}_{\mathbf{y}|\mathbf{x}; \phi, \theta} [-\log p(\mathbf{a}|\mathbf{y})]] \\
 & \leq \mathbb{E}_{\mathbf{a}, \mathbf{x}} [\mathbb{E}_{\mathbf{y}|\mathbf{x}; \phi, \theta} [-\log q_{\psi}(\mathbf{a}|\mathbf{y})]].
 \end{aligned}$$

APPENDIX B  
DERIVATION OF (33)

Since we assume  $q_\psi(\mathbf{a}|\mathbf{y})$  takes on a Gaussian distribution  $\mathcal{N}(\boldsymbol{\mu}_\psi(\mathbf{y}), \boldsymbol{\Sigma}_\psi(\mathbf{y}))$ , where  $\boldsymbol{\Sigma}_\psi(\mathbf{y}) = \sigma_c^2 \mathbf{I}_d$ , the simplification process is shown below:

$$\begin{aligned} & -\log q_\psi(\mathbf{a}|\mathbf{y}) \\ &= -\log \mathcal{N}(\boldsymbol{\mu}_\psi(\mathbf{y}), \boldsymbol{\Sigma}_\psi(\mathbf{y})) \\ &= -\log \left[ \exp \left( -\frac{1}{2} (\mathbf{a} - \boldsymbol{\mu}_\psi(\mathbf{y}))^T \boldsymbol{\Sigma}_\psi^{-1}(\mathbf{y}) (\mathbf{a} - \boldsymbol{\mu}_\psi(\mathbf{y})) \right) \right] \\ & \quad + \log \left[ (2\pi)^{\frac{d}{2}} |\boldsymbol{\Sigma}_\psi(\mathbf{y})|^{\frac{1}{2}} \right] \\ &= \frac{\|\mathbf{a} - \boldsymbol{\mu}_\psi(\mathbf{y})\|_2^2}{2\sigma_c^2} + d \log \sigma_c + \frac{d}{2} \log 2\pi. \end{aligned}$$

Since  $\sigma_c$  is a constant, we have

$$-\log q_\psi(\mathbf{a}|\mathbf{y}) \sim \frac{1}{2\sigma_c^2} \|\mathbf{a} - \boldsymbol{\mu}_\psi(\mathbf{y})\|_2^2.$$

REFERENCES

- [1] T. M. Cover and J. A. Thomas, *Elements of Information Theory*, Second edition. New York, NY, USA, 1991.
- [2] E. Bourtsoulatzé, D. Burth Kurka, and D. Gündüz, "Deep joint source-channel coding for wireless image transmission," *IEEE Trans. on Cogn. Commun. Netw.*, vol. 5, no. 3, pp. 567–579, 2019.
- [3] D. B. Kurka and D. Gündüz, "DeepJSCC-f: Deep joint source-channel coding of images with feedback," *IEEE J. Sel. Areas Inf. Theory*, vol. 1, no. 1, pp. 178–193, 2020.
- [4] J. Shao, Y. Mao, and J. Zhang, "Learning task-oriented communication for edge inference: An information bottleneck approach," *IEEE J. Sel. Areas Commun.*, vol. 40, no. 1, pp. 197–211, 2022.
- [5] J. Shao, Y. Mao, and J. Zhang, "Task-oriented communication for multi-device cooperative edge inference," *IEEE Trans. Wireless Commun.*, vol. 22, no. 1, pp. 73–87, 2023.
- [6] P. A. Stavrou and M. Kountouris, "A rate distortion approach to goal-oriented communication," in *Proc. IEEE Int. Symp. Inf. Theory*, 2022, pp. 590–595.
- [7] Y. Shi, Y. Zhou, D. Wen, Y. Wu, C. Jiang, and K. B. Letaief, "Task-oriented communications for 6G: Vision, principles, and technologies," *IEEE Wirel. Commun.*, vol. 30, no. 3, pp. 78–85, 2023.
- [8] J. Zhang and K. B. Letaief, "Mobile edge intelligence and computing for the internet of vehicles," *Proc. IEEE*, vol. 108, no. 2, pp. 246–261, 2020.
- [9] S. Liu, L. Liu, J. Tang, B. Yu, Y. Wang, and W. Shi, "Edge computing for autonomous driving: Opportunities and challenges," *Proc. IEEE*, vol. 107, no. 8, pp. 1697–1716, 2019.
- [10] E. Li, Z. Zhou, and X. Chen, "Edge intelligence: On-demand deep learning model co-inference with device-edge synergy," in *Proc. Workshop Mobile Edge Commun.*, ser. MECOMM'18, Budapest, Hungary, 2018, pp. 31–36.
- [11] M. Jankowski, D. Gündüz, and K. Mikolajczyk, "Wireless image retrieval at the edge," *IEEE J. Sel. Areas Commun.*, vol. 39, no. 1, pp. 89–100, 2021.
- [12] J. Shao and J. Zhang, "BottleNet++: An end-to-end approach for feature compression in device-edge co-inference systems," in *Proc. IEEE Int. Conf. Commun. Workshops*, 2020, pp. 1–6.
- [13] M. Jankowski, D. Gündüz, and K. Mikolajczyk, "Joint device-edge inference over wireless links with pruning," in *Proc. IEEE Int. Workshop Signal Process. Adv. Wireless Commun.*, 2020, pp. 1–5.
- [14] D. B. Kurka and D. Gündüz, "Successive refinement of images with deep joint source-channel coding," in *Proc. IEEE Int. Workshop Signal Process. Adv. Wireless Commun.*, 2019, pp. 1–5.
- [15] G. Wallace, "The JPEG still picture compression standard," *IEEE Trans. Consum. Electron.*, vol. 38, no. 1, pp. 18–34, 1992.
- [16] D. S. Taubman, M. W. Marcellin, and M. Rabhani, "JPEG2000: Image compression fundamentals, standards and practice," *J. Electron. Imag.*, vol. 11, no. 2, pp. 286–287, 2002.
- [17] R. Gallager, "Low-density parity-check codes," *IRE Trans. Inf. Theory*, vol. 8, no. 1, pp. 21–28, 1962.
- [18] T.-Y. Tung, D. B. Kurka, M. Jankowski, and D. Gündüz, "DeepJSCC-Q: Constellation constrained deep joint source-channel coding," *IEEE J. Sel. Areas Inf. Theory*, vol. 3, no. 4, pp. 720–731, 2022.
- [19] M. Yang, C. Bian, and H.-S. Kim, "OFDM-guided deep joint source channel coding for wireless multipath fading channels," *IEEE Trans. Cogn. Commun. Netw.*, vol. 8, no. 2, pp. 584–599, 2022.
- [20] T.-Y. Tung and D. Gündüz, "Deep-learning-aided wireless video transmission," in *Proc. IEEE Int. Workshop Signal Process. Adv. Wireless Commun.*, 2022, pp. 1–5.
- [21] C. Chaccour, W. Saad, M. Debbah, Z. Han, and H. V. Poor, "Less data, more knowledge: Building next generation semantic communication networks," *IEEE Commun. Surv. Tut.*, pp. 1–1, 2024.
- [22] W. Yang, H. Du, Z. Q. Liew, et al., "Semantic communications for future internet: Fundamentals, applications, and challenges," *IEEE Commun. Surv. Tut.*, vol. 25, no. 1, pp. 213–250, 2023.
- [23] Z. Qin, X. Tao, J. Lu, W. Tong, and G. Y. Li, "Semantic communications: Principles and challenges," *arXiv preprint arXiv:2201.01389*, 2021.
- [24] E. C. Strinati, P. Di Lorenzo, V. Sciancalepore, et al., "Goal-oriented and semantic communication in 6G AI-native networks: The 6G-GOALS approach," *arXiv preprint arXiv:2402.07573*, 2024.
- [25] S. R. Pandey, V. P. Bui, and P. Popovski, "Goal-oriented communications in federated learning via feedback on risk-averse participation," in *Proc. IEEE Int. Symp. Pers. Indoor Mob. Radio Commun.*, 2023, pp. 1–6.
- [26] J. Kang, H. Du, Z. Li, et al., "Personalized saliency in task-oriented semantic communications: Image transmission and performance analysis," *IEEE J. Sel. Areas Commun.*, vol. 41, no. 1, pp. 186–201, 2023.
- [27] H. Xie, Z. Qin, G. Y. Li, and B.-H. Juang, "Deep learning enabled semantic communication systems," *IEEE Trans. Signal Process.*, vol. 69, pp. 2663–2675, 2021.
- [28] N. Farsad, M. Rao, and A. Goldsmith, "Deep learning for joint source-channel coding of text," in *Proc. IEEE Int. Conf. Acoust., Speech, Signal Process.*, 2018, pp. 2326–2330.
- [29] Q. Hu, G. Zhang, Z. Qin, Y. Cai, G. Yu, and G. Y. Li, "Robust semantic communications against semantic noise," in *Proc. IEEE Veh. Technol. Conf.*, 2022, pp. 1–6.
- [30] Y. Diao, Z. Meng, X. Xu, C. She, and P. G. Zhao, "Task-oriented source-channel coding enabled autonomous driving based on edge computing," in *Proc. IEEE Conf. Comput. Commun. Workshops*, 2024, pp. 1–6.
- [31] Y. Diao, Y. Zhang, P. G. Zhao, and D. De Martini, "TAGIC: Task-guided image communication framework for seamless teleoperation," in *Proc. IEEE Conf. Comput. Commun. Workshops*, 2024, pp. 1–2.
- [32] Y. Shao and D. Gündüz, "Semantic communications with discrete-time analog transmission: A PAPR perspective," *IEEE Wireless Commun. Lett.*, vol. 12, no. 3, pp. 510–514, 2023.
- [33] "IEEE standard for low-rate wireless networks," *IEEE Standard 802.15.4-2020*, pp. 1–800, 2020.
- [34] K. Choi, K. Tatwawadi, A. Grover, T. Weissman, and S. Ermon, "Neural joint source-channel coding," in *Proc. Int. Conf. Mach. Learn.*, ser. Proceedings of Machine Learning Research, vol. 97, 2019, pp. 1182–1192.
- [35] Y. Song, M. Xu, L. Yu, H. Zhou, S. Shao, and Y. Yu, "Infomax neural joint source-channel coding via adversarial bit flip," in *Proc. AAAI Conf. Artif. Intell.*, vol. 34, 2020, pp. 5834–5841.
- [36] T.-Y. Tung, D. B. Kurka, M. Jankowski, and D. Gündüz, "DeepJSCC-Q: Channel input constrained deep joint source-channel coding," in *Proc. IEEE Int. Conf. Commun.*, 2022, pp. 3880–3885.
- [37] W. Hu, Y. Yang, Y. C. Eldar, C. Feng, and C. Guo, "Digital task-oriented communication with hardware-limited task-based quantization," in *Proc. IEEE Int. Conf. Acoust., Speech, Signal Process.*, 2024, pp. 171–175.
- [38] Y. Shi, K. Yang, T. Jiang, J. Zhang, and K. B. Letaief, "Communication-efficient edge AI: Algorithms and systems," *IEEE Commun. Surv. Tut.*, vol. 22, no. 4, pp. 2167–2191, 2020.
- [39] X. Huang and S. Zhou, "Dynamic compression ratio selection for edge inference systems with hard deadlines," *IEEE Internet Things J.*, vol. 7, no. 9, pp. 8800–8810, 2020.
- [40] W. Shi, Y. Hou, S. Zhou, Z. Niu, Y. Zhang, and L. Geng, "Improving device-edge cooperative inference of deep learning via 2-step pruning," in *Proc. IEEE Conf. Comput. Commun. Workshops*, 2019, pp. 1–6.
- [41] E. Li, L. Zeng, Z. Zhou, and X. Chen, "Edge AI: On-demand accelerating deep neural network inference via edge computing," *IEEE Trans. Wireless Commun.*, vol. 19, no. 1, pp. 447–457, 2020.

- [42] J. Shao and J. Zhang, "Communication-computation trade-off in resource-constrained edge inference," *IEEE Commun. Mag.*, vol. 58, no. 12, pp. 20–26, 2020.
- [43] Y. Dubois, B. Bloem-Reddy, K. Ullrich, and C. J. Maddison, "Lossy compression for lossless prediction," in *Proc. Adv. Neural Inf. Process. Syst.*, vol. 34, 2021, pp. 14 014–14 028.
- [44] J. Shao, H. Zhang, Y. Mao, and J. Zhang, "Branchy-GNN: A device-edge co-inference framework for efficient point cloud processing," in *Proc. IEEE Int. Conf. Acoust., Speech, Signal Process.*, 2021, pp. 8488–8492.
- [45] N. Tishby, F. C. Pereira, and W. Bialek, "The information bottleneck method," in *Proc. Annu. Allerton Conf. Commun. Control Comput.*, 1999, pp. 368–377.
- [46] N. Tishby and N. Zaslavsky, "Deep learning and the information bottleneck principle," in *Proc. IEEE Inf. Theory Workshop*, 2015, pp. 1–5.
- [47] S. Arimoto, "An algorithm for computing the capacity of arbitrary discrete memoryless channels," *IEEE Trans. Inf. Theory*, vol. 18, no. 1, pp. 14–20, 1972.
- [48] R. Blahut, "Computation of channel capacity and rate-distortion functions," *IEEE Trans. Inf. Theory*, vol. 18, no. 4, pp. 460–473, 1972.
- [49] A. A. Alemi, I. Fischer, J. V. Dillon, and K. Murphy, "Deep variational information bottleneck," in *Proc. Int. Conf. Learn. Represent.*, 2017.
- [50] H. Wei, W. Ni, W. Xu, F. Wang, D. Niyato, and P. Zhang, "Federated semantic learning driven by information bottleneck for task-oriented communications," *IEEE Commun. Lett.*, vol. 27, no. 10, pp. 2652–2656, 2023.
- [51] L. Sun, Y. Yang, M. Chen, and C. Guo, "Disentangled information bottleneck guided privacy-protective joint source and channel coding for image transmission," *IEEE Trans. Commun.*, pp. 1–1, 2024.
- [52] P. Wu, X. Jia, L. Chen, J. Yan, H. Li, and Y. Qiao, "Trajectory-guided control prediction for end-to-end autonomous driving: A simple yet strong baseline," in *Proc. Adv. Neural Inf. Process. Syst.*, vol. 35, 2022, pp. 6119–6132.
- [53] D. P. Kingma and M. Welling, "Auto-encoding variational bayes," *arXiv preprint arXiv:1312.6114*, 2013.
- [54] J. Duchi, "Derivations for linear algebra and optimization," 2007.
- [55] Z. Zhang, A. Liniger, D. Dai, F. Yu, and L. Van Gool, "End-to-end urban driving by imitating a reinforcement learning coach," in *Proc. Int. Conf. Comput. Vis.*, 2021, pp. 15 222–15 232.
- [56] A. Dosovitskiy, G. Ros, F. Codevilla, A. Lopez, and V. Koltun, "CARLA: An open urban driving simulator," in *Proc. Annu. Conf. Robot Learn.*, ser. Proceedings of Machine Learning Research, vol. 78, 2017, pp. 1–16.
- [57] F. Bellard. "BPG image format." (2014), [Online]. Available: <https://bellard.org/bpg/>.
- [58] Y. M. Saidutta, A. Abdi, and F. Fekri, "Joint source-channel coding over additive noise analog channels using mixture of variational autoencoders," *IEEE J. Sel. Areas Commun.*, vol. 39, no. 7, pp. 2000–2013, 2021.